

Flow Analysis between Two Bluff Bodies in a Close Distance Platooning Configuration

van Tilborg, Frank; Van Raemdonck, Gandert; Sciacchitano, Andrea; Casalino, Damiano

DOI

[10.4271/02-12-03-0015](https://doi.org/10.4271/02-12-03-0015)

Publication date

2019

Document Version

Accepted author manuscript

Published in

SAE International Journal of Fuels and Lubricants

Citation (APA)

van Tilborg, F., Van Raemdonck, G., Sciacchitano, A., & Casalino, D. (2019). Flow Analysis between Two Bluff Bodies in a Close Distance Platooning Configuration. *SAE International Journal of Fuels and Lubricants*, 12(3), 179-196. <https://doi.org/10.4271/02-12-03-0015>

Important note

To cite this publication, please use the final published version (if applicable).
Please check the document version above.

Copyright

Other than for strictly personal use, it is not permitted to download, forward or distribute the text or part of it, without the consent of the author(s) and/or copyright holder(s), unless the work is under an open content license such as Creative Commons.

Takedown policy

Please contact us and provide details if you believe this document breaches copyrights.
We will remove access to the work immediately and investigate your claim.

Green Open Access added to TU Delft Institutional Repository

'You share, we take care!' - Taverne project

<https://www.openaccess.nl/en/you-share-we-take-care>

Otherwise as indicated in the copyright section: the publisher is the copyright holder of this work and the author uses the Dutch legislation to make this work public.

Flow analysis between two bluff bodies in a close distance platooning configuration

Frank van Tilborg - Technische Universiteit Delft, The Netherlands , Gandert Van Raemdonck - Technische Universiteit Delft, The Netherlands , Andrea Sciacchitano - Technische Universiteit Delft, The Netherlands , Damiano Casalino - Technische Universiteit Delft, The Netherlands

Abstract

This paper analyses the flowfield between two Generalized European Transport System (GETS) models which are placed in a two-vehicle platoon at close distances. Numerical simulations using the Lattice Boltzmann method implemented in Exa's software package together with a windtunnel experiment (open jet facility) were executed. Next to balance measurements Coaxial Volumetric velocimetry (CVV) measurements were performed to obtain information about the flowfield. Three intervehicle distances for various platoon configurations were tested where the vehicles in the platoon varied in terms of front edge radius and the addition of tails. At the smallest intervehicle distance the greatest reductions in drag were found for both the leading and trailing vehicle. The flow in the gap between the two vehicles follows an S-shaped path with small variations between the configurations. For the second distance the leading model still sees a decrease in drag however smaller compared to the closest distance. For the trailing model either a drag increase or decrease is seen depending on its front edge radius. The addition of a tail to the trailing model always benefits the drag reduction, applying a tail to the leading model can be both beneficial and disadvantageous to the drag of the trailing model depending on the tail angle. The wake of the leading model resembles that of the isolated model again. Due to the vortex shedding of the leading model large fluctuations in force are seen for the trailing model. At the largest distance the drag decrease for the leading model is on the order of a few percent, for the trailing model this again depends on the front edge radius. At this distance the wake of the leading model has returned to that of the isolated model.

Introduction

In the European Union CO₂ emissions make up 30% of all on-road transport [1]. This share is expected to grow to 45% by the year 2030 [2]. At highway speeds more than 40% of fuel consumption is spent overcoming aerodynamic drag [3]. At higher speeds this percentage grows even further. Most of this aerodynamic drag is generated by the front and rear region of the vehicle. In the front the air collides with the vehicle resulting in a high-pressure field pushing the vehicle back. In the rear the vehicle draws a region of air with it resulting in a low-pressure region.

One way to reduce the aerodynamic drag is by streamlining heavy duty vehicles by using drag reductions devices such as: tractor-trailer gap devices, trailer skirts and boat-tails.

The effect of these has been shown by many studies such as the one done by Mcauliffe [4]. Here five different boat-tails all with an angle of 13° on a 30% realistic scale model were tested. Drag reduction of these was between 5.7% and 6.8%. Van Raemdonck [5] tested boat-tails with varying angles and reduced the drag by 30% for a fully closed tail at 12°. For even longer tails 40% drag reduction was achieved. Next to experiments numerical studies have also been done. Hyams et al. [6] used unsteady RANS simulations on a Generic Conventional Model where a tail of 15° was applied. For this study a 15% wind averaged drag reduction was found.

Aerodynamic drag can also be reduced by platooning which is the act of vehicles driving close to each other such that the trailing vehicle drives in the wake of the leading one. Both vehicles benefit from this situation because the pressure in the wake of the leading vehicle increases while the stagnation pressure on the front of the trailing vehicle decreases.

Hammache and Browand [7] investigated the effect of platooning on two truck-like models with either a rounded or sharp front end. At small separation distances the leading vehicle drag reduction is between 30% and 10% depending on the type of front end. For the trailing vehicle the reductions are even higher 60% for the sharp and 80% for the rounded front. At larger distances the drag reductions diminish. Mihelic et al. [8] performed a numerical study on realistic truck models. At a separation distance of 9.14 m the drag of the lead vehicle decreased with 12% and that of the trailing one with 14%. Gheysens [9] studied the effect of drag reduction devices consisting of front edge radius and the application of a boat tail, on a 3 vehicle platoon. Time averaged simulations showed that changing the front edge radius had a big influence. For larger radii the drag increased while for smaller radii the opposite was true. For smaller inter-vehicle distances the lead vehicle experienced large drag reductions due to the high pressure region from the middle vehicle. The trailing vehicle drag increased for decreasing inter-vehicle distances because of the inward deflection of the streamlines coming from the middle vehicle. The drag of the middle vehicle remained constant experiencing both effects from the lead and trailing vehicle. When tails were added or had more inward deflection the drag reduction decreased.

The literature shows that there is a great interest in reducing the drag of heavy duty vehicles by platooning. Most of them only present the drag reductions and do not disclose what happens to the flowfield which is what this study aims to do. In addition to this the flow behavior with intervehicle distance, effect of rear and front body modifications and unsteady wake flow will also be investigated.

Numerical Setup

For the numerical simulations the package of Exa's PowerFLOW was used which makes use of the lattice Boltzmann method. This method is based on the kinetic theory of gases and instead of directly calculating macroscopic variables such as velocity and pressure it models the interaction of molecules. The problem is expressed by a one-body distribution function $f(x,v,t)$ which indicates the density of particles at a given position x , velocity v and time t . The resulting Boltzmann equation is given by equation 1 [10].

$$Df = \frac{\partial f}{\partial t} + \mathbf{v} \cdot \frac{\partial f}{\partial \mathbf{x}} = C(f, f) \quad (1)$$

In this equation the left-hand side represents the free-streaming of the molecules in space and time while the right-hand side covers the complex interactions and collisions between molecules. To calculate this term PowerFLOW uses the Bhatnagar-Gross-Krook (BGK) collision term operator [11]. The particle distribution is calculated by solving the kinetic equations on a Cartesian mesh. On this Cartesian mesh particles can move in three dimensions using 19 discrete velocities better known as the D3Q19 model.

Because of the high Reynolds number it is not feasible to use direct simulation to resolve all the scales of motion. That is why turbulence modelling must be used. PowerFLOW uses very large eddy simulation (VLES) together with a κ - ϵ Renormalization group (RNG) for the smaller unresolved scales [12].

The model used for the simulations and the experimental campaign is the 1/8 scale Generalized European Transport System model which is an abstraction of a European truck model. The model is illustrated in figure 1.

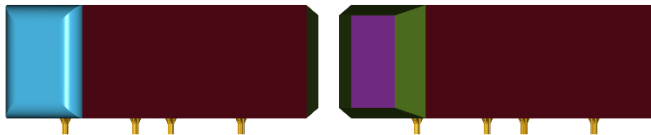


Figure 1. GETS Model, front view on the left and rear view on the right where different parts have different colors. Blue indicates the front, purple the rear, the sides are maroon while the tail is colored green. Lastly the supports are yellow.

Throughout this study two parts of this model were varied namely the front radius (in blue) and the boat-tail (in green). Around this model the simulation volume was created next in which the flow was calculated. The dimensions of this volume are eleven times the length of the model, three upstream and seven downstream. The width is ten times the model width and the height is six times the model height. The dimensions of this simulation volume were based on the recommendations of SAE [13]. To resemble the experimental setup as much as possible a ground plate was placed under the model.

To ensure enough spatial resolution two more regions were created around the model which are visible in figure 2. The region in red is a

5 mm offset and the blue box has a length of 1.6 times the model length. 10% of the model length is placed upstream and 50% is placed downstream of the model. The width and height of this wakebox is 1.2 and 1.3 times the width and height of the model. The offset contains a lattice with a size of 1.25 mm and the wakebox one of 2.5 mm.

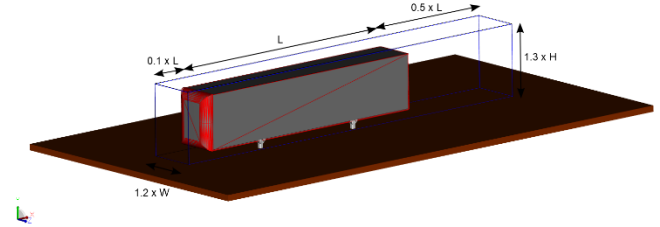


Figure 2. GETS model with additional regions for extra spatial resolution.

The rest of the simulation volume is filled up with a larger sized lattice where the biggest one is 320 mm farthest away from the model. These lattice sizes were obtained by performing a lattice sensitivity study [14].

Experimental Setup

Next to the numerical simulations an experimental campaign was held in the Open Jet Facility (OJF) wind tunnel at the faculty of Aerospace Engineering, TU Delft. The wind velocity in the open test section was 15 m/s which is the same as was used for the simulations. Besides force measurements using a balance provided by NLR [15], information about the flowfield was captured using Coaxial Volumetric Velocimetry (CVV). The experimental setup for this can be regarded in figure 3.

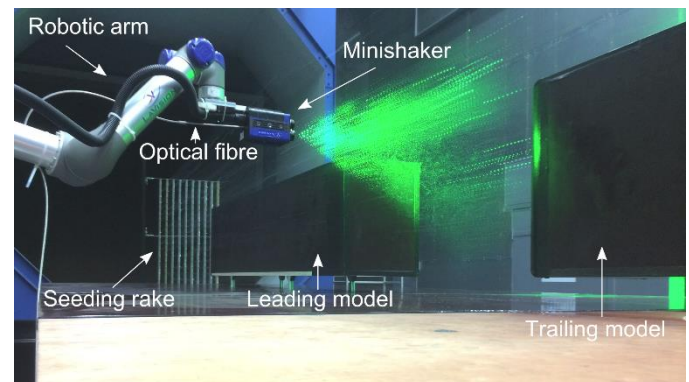


Figure 3. Experimental setup for the CVV measurements.

This method has some advantages over conventional tomographic PIV which will be explained here together with the necessary hardware.

For these CVV measurements the flow was seeded with helium filled soap bubbles (HFSB) introduced by Scarano et al. [16] which allow for a large measurement volume with reduced illumination intensity. The bubbles are produced by the seeding rake visible in figure 3 which is made up of 10 wings containing 20 nozzles each. Each of the nozzles nominally produces 30,000 HFSB per second and the bubble production is regulated by a *LaVision* Fluid Supply Unit. The bubbles flow into the gap between the two models where they are illuminated by laser light coming from a *Quantronix Darwin Duo Nd:YLF* high speed laser. This laser light comes through the optical

fiber which is housed inside the cuboid which also houses four *LaVision MiniShaker S* CMOS cameras with protruding lenses. The cameras have a sensor size of 800 x 600 pixels however because of the velocity of 15 m/s this had to be reduced to have a higher image rate of 749 Hz. For this image rate the sensor size reduces to 720 x 432 pixels. Because the four cameras do not move with respect to each other during operation, geometrical calibration only once for the experimental campaign and in theory for the lifetime of the Minishaker. Details about this calibration can be found in [17]. Next to the geometrical calibration a volume self-calibration is done as well to improve the accuracy of the system [18]. Because the imaging and illumination is all contained in the Minishaker and was placed upon a *Universal Robots - UR5* robotic arm it was very easy to position it in the gap between the two models.

The images coming from the experiment were further processed to obtain the velocity using the Shake the Box algorithm [19]. This algorithm is implemented in *Davis 8.4.0* and uses Iterative Particle Reconstruction with particle prediction. For more information on the concepts used in this algorithm the user is directed to [20] and [19].

Results

Single Configurations

Baseline Configuration

The first results that are presented are the ones coming from the baseline configuration where the GETS model has a front radius of 68 mm for the 1/8 scale. In figure 4 the drag contributions and total drag coefficients are given from results obtained in this study as well as ones from previous work.

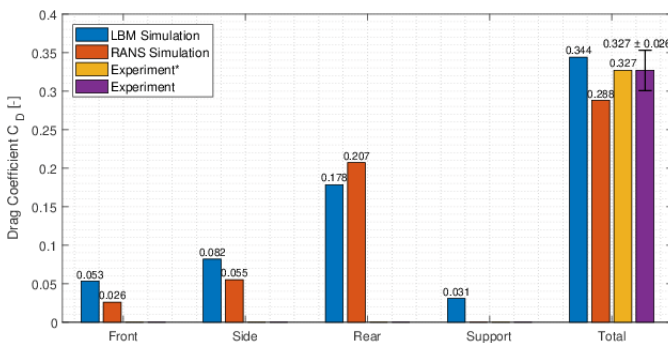


Figure 4. Numerical drag distribution and experimental total drag coefficients for the baseline configuration, RANS simulation data from [9] and experimental* data obtained from [21].

Whereas this study used a model of scale 1/8 this cannot be said for all results in figure 4. The results from Gheysens [9] were obtained for a full-scale model with no supports and a moving floor which was tested at a Re of 5.1×10^6 Van Raemdonck and Van Tooren [21] performed a wind tunnel experiment on a 1/15 scale model at a Reynolds number of 8.3×10^5 .

The drag coefficients coming from PowerFLOW and the experiment performed in this study agree very well. The difference is only 17 counts (5%) which is in the error bar. The agreement between the two experiments is also excellent, both show a C_D of 0.327. The first thing that can be seen when looking at Gheysens' [9] results is that the total drag coefficient is lower which is partly due to the lack of supports. When considering the drag distribution in figure 4 the front

drag is about half of that given by PowerFLOW. This is due to the increased suction generated by the front edges at higher flow speeds. The side drag is also lower, this is due to the lowered shear stress because of the thicker boundary layer at higher x-position. Lastly the rear drag is higher than that of the LBM simulation which can be explained by looking at the base pressure given in figure 5.

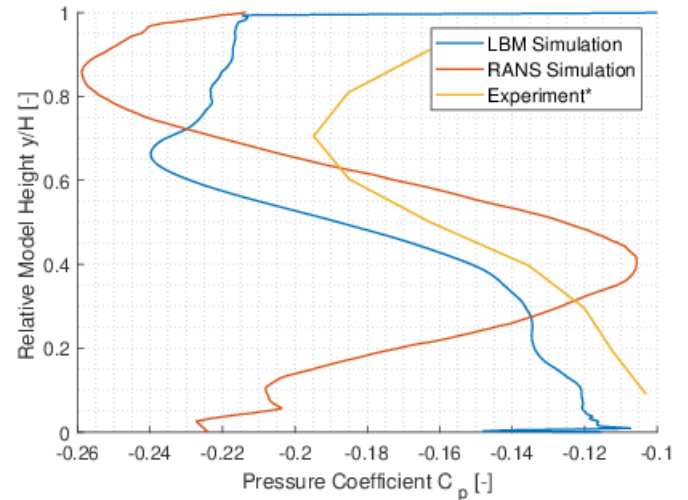


Figure 5. Numerical and experimental base pressure distribution, RANS simulation data from [9] and experimental* data obtained from [21].

The base pressure from the RANS simulation is much lower for the top and bottom quarter compared to the pressure coming from PowerFLOW. The most positive peak also has a much higher magnitude. The shape of the experimental pressure distribution from Van Raemdonck and Van Tooren [21] is very similar to the one coming from PowerFLOW.

This pressure distribution comes from the wake that is formed at the back of the GETS model which is shown in figure 6. In this figure we can see that the wake is made up of two main vortices where the upper one has a larger suction effect than the lower one because its location is closer to the model.

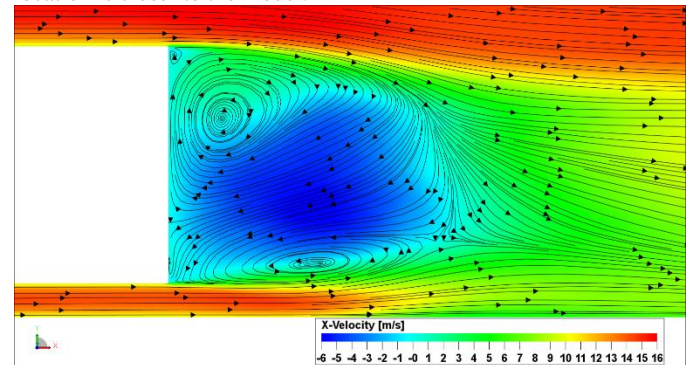


Figure 6. Time-averaged wake structure for the baseline GETS model, streamlines with contours of x-velocity from PowerFLOW results.

In general, the flow enters the wake from the top or bottom and flows into one of the two main vortices it then either stagnates on the rear surface of the model or flows further downstream and leaves the wake. Vortex shedding is one of the phenomena that occurs in the wake and it affects the transient forces of the model. In figure 7 the power spectrum density (PSD) plot for the drag side and lift force is given.

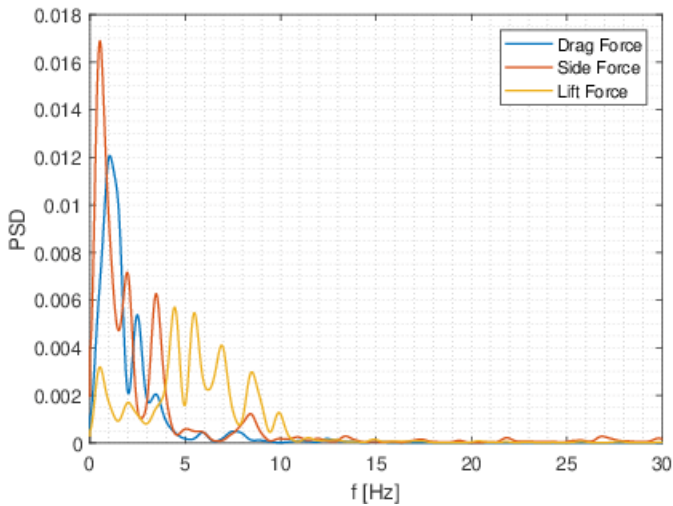


Figure 7. PSD of the forces of the baseline model, PowerFLOW.

From the figure it can be seen that the drag forces fluctuates at a Strouhal number of 0.073 which is comparable to the values found by Khalighi et al. [22] and Krajnović and Davidson [23] from unsteady base pressure analyses. For the side and lift force multiple peaks of roughly the same amplitude can be seen. These are located at a Strouhal number of 0.058 and 0.102 for the side force and 0.130 and 0.160 for the lift force.

Effect of Front Edge Radius

The first variation on the presented baseline configuration is the effect of a sharper leading edge radius. The radius is halved two times. In figure 8 the drag coefficients for these configurations are given from both simulation and experimental data.

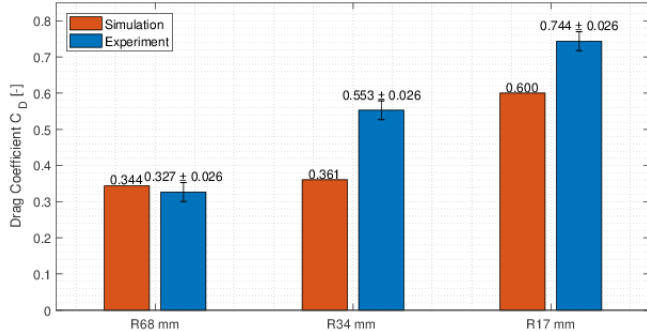


Figure 8. Drag coefficient for the GETS model with different leading edge radii.

While considering the numerical result one can observe that the drag increases with 17 counts when the radius is halved a first time and then with 234 counts when it is halved a second time. This is not comparable to the results from the experiment there the first drag increase is much higher (226 counts) and 191 counts for the sharpest radius. This difference in drag is due to the prediction of leading edge flow separation in PowerFLOW. In the wind tunnel experiment for the middle radius leading edge flow separation was noted, while this did not occur in the simulation as is shown in figure 9. For the sharpest radius separation was seen in both the simulation and the experiment but it is thought that it is not as severe for the simulation which leads to the lower drag.

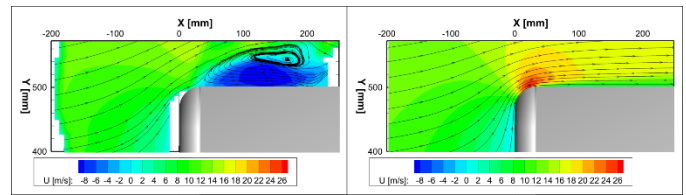


Figure 9. Numerical drag distribution for the GETS model with different front edge radii.

While the simulation does not perfectly model the separation at the front of the model it is still worth looking at the drag distribution of the various parts given in figure 10. As was stated before when halving the radius once the drag difference is only 17 counts. However there is quite some difference how the drag is split up.

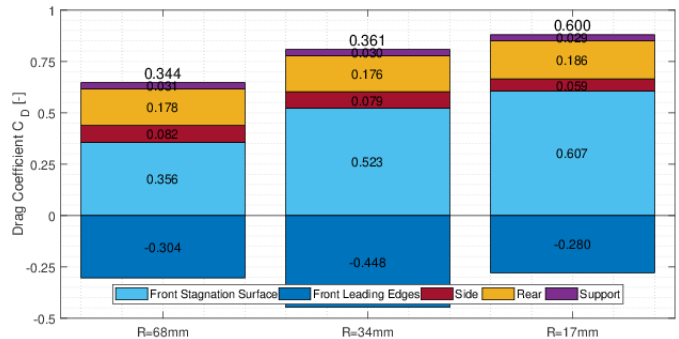


Figure 10. Numerical drag distribution for the GETS model with different front edge radii.

Going from a leading edge radius of 68 mm to 34 mm 167 counts are added to the front stagnation surface due to its larger size. Because of the sharper edges the flow is accelerated more which leads to a higher suction force leading to 144 more thrust counts. The model where the sharpest radius ($R = 17\text{mm}$) is applied has a high drag increase due to the loss of suction caused by separation and due to the increase in the frontal surface area. Besides the changes caused by the frontal area shaping some differences can also be seen in the drag generated by the side and rear. For the drag caused by the rear surface when the radius is halved a first time the drag is reduced by 2 counts. Due to the thicker boundary layer caused by the smaller radius of the front leading edges the pressure at the rear reduces and thus with it the drag caused by the rear. This behavior was also seen by Van Raemdonck [5] and Gheysens [9] from the results of a wind tunnel test and numerical simulation respectively.

Effect of Tails

The last alteration applied on the single vehicle is the addition of a tail. Tails with three different angles were added to the baseline GETS model. One of 0°, 6° and 12°. In figure 11 the drag decreases for each tail is given both numerically and experimentally.

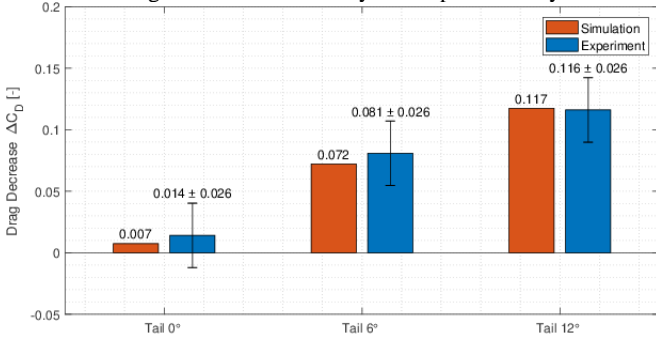


Figure 11. Drag coefficient reductions for various tail configurations: $\Delta C_D = C_{D, \text{baseline}} - C_{D, \text{tail}}$.

When a straight tail of 0° is applied the drag coefficient decreases with 7 counts (2%) and 14 counts (4%) for the simulation and experiment respectively. For the tail of 6° the reduction becomes even larger 72 counts (21%) for the simulation and 81 counts (25%) for the experiment. The final tail of 12° that was applied results in drag decreases of 117 counts (34%) and 116 counts (35%) for the simulation and experiment. From this analysis it can be noticed that the results from the simulation and the experiment agree very well. The differences between simulation and experiment are rather small and all fall in the error bar of the experiment. Next to this the trend of the various tails for the simulation and experiment is very similar.

The effect of tails was also investigated by Gheysens [9] and Van Raemdonck [5] using RANS simulations on a full scale GETS model and a wind tunnel experiment on a 1/15 scale GETS model respectively. The resulting drag decrease was 15 (5%), 87 (29%) and 124 counts (41%) for the tails with increasing angles from the simulation and 90 drag counts (28%) for the tail of 12°, although its length was 30% shorter than the one applied in this study, from the wind tunnel experiment.

From this it can be said that the effectiveness of a tail increases with Reynolds number which was also found by Van Raemdonck [5]. This is because the pressure drag is proportional to the Reynolds number. Because the tail works by decreasing the negative pressure at the rear of the model the addition of a tail will have a larger effect on the drag a higher Reynolds numbers.

Next to the drag the tail also reduces the fluctuations in the wake of the model. This can be seen when looking at figure 12 which show the PSD of the drag and sideforce for the different tails.

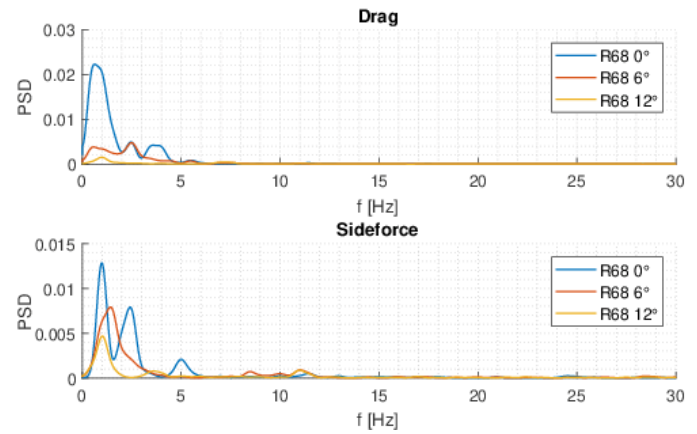


Figure 12. PSD of the drag and sideforce of the model with various tails applied, PowerFLOW.

In general it can be seen that the fluctuations diminish with increasing tail angle. Lower fluctuations with a stepped tail were also reported by Khalighi et al. [22] for a stepped tail. Looking at the drag force for the model where a tail of 0° and 6° is applied a peak exists at a Strouhal number of 0.071 no peak can be seen for the tail of 12°. The side force also shows a peak at the same Strouhal number for the model with a tail of 0°. For the other models no peak at this number can be seen although peaks at lower frequencies can be seen which for the tail of 12° shows a lower amplitude.

Platoon Configurations

Several platoon configurations at three intervehicle distances were tested. These distances s were normalized with the model length L and are 0.1, 0.45 and 0.9. These distances were chosen because from a previous study [24] it was seen that there is a lot of variation in the fuel saving at small intervehicle distances.

Smallest intervehicle distance: 0.10 s/L

At the smallest intervehicle distance two configurations were analyzed namely the baseline platoon where both vehicles have the bluntest front edge radius of 68 mm and one where the trailing model has the sharpest radius of 17 mm. In figure 13 the relative and absolute drag coefficient for the two tested configurations plus an additional one where the trailing model was misaligned 10 mm in the vertical direction. This was done because a similar alignment issue occurred during the wind tunnel test and proved very difficult to get rid of in the timespan of the experiment.

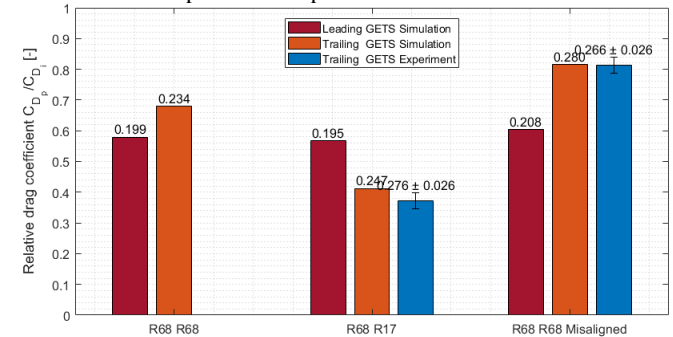


Figure 13. Numerical and experimental drag coefficient for the platoons at 0.10 s/L.

From the simulation data all configurations benefit at this distance. The baseline R68-R68 configuration loses 42% and 32% for the leading and trailing vehicle. For the R68-R17 configuration the drag is even lower. The drag reduction is 43% and 59%. In this case the trailing model loses most of the drag which was also found by Hammache and Browand [7]. For the misaligned case the drag increases slightly here only 40% and 18% drag is reduced.

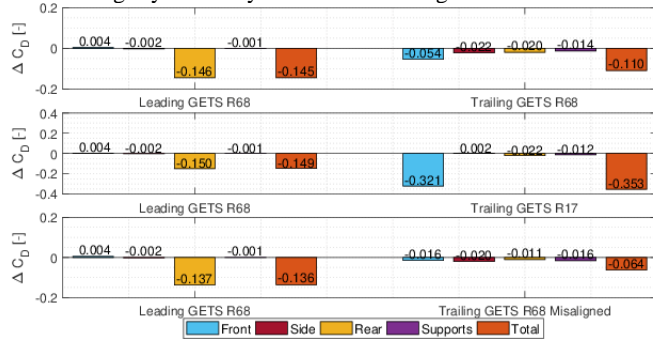


Figure 14. Numerical drag differences with respect to the single model for the leading and trailing model in a platoon at 0.10 s/L.

From figure 14 where the differences in drag are given the highest losses are coming from the rear of the leading model and the front of the trailing model. This is to be expected because of the way the pressure fields from the rear and front influence each other which will be explained further on.

For the experimental data only forces were obtained on the trailing model also here for all configurations one can regard a drag decrease which is slightly higher compared to the simulation data. For the R68-R17 platoon the drag is decreased by 63%. The absolute difference is 33 drag counts which just falls out of the error bar. The difference in relative drag coefficient is a combination of the error in the drag of the single model and that of the platoon. The mismatch between the absolute drag coefficient is caused by a slight vertical alignment error that was also seen in the platoon where both models had the largest front radius. For this misaligned platoon the drag decrease is 20% and the absolute differences is 14 counts which falls well within the error bar.

These drag decreases are caused by the altered flowfield which exists between the two models. Information about this flowfield was obtained in both simulation and experiment and is visible in figure 15 for the R68-R68 configurations.

From this figure the general flow in the gap can be described. Most of the flow is entering from the bottom of the model. As it enters the gap it decelerates and ends up into the lower vortex of low pressure that exists in the model. Part of it does not enter this vortex and stagnates on the lower rounded edge which creates a high pressure. The flow that is not contained in this vortex continues its way upward where some of it stagnates on the rear surface of the leading model creating higher pressure. The rest of the flow moves further upward where it either enters the low pressure top vortex or stagnates on the rounded edge and leaves the gap. This flow pattern causes a higher base pressure on the leading vehicle especially in the stagnation region and a lowered stagnation pressure on the trailing model. Next to this the suction that is produced by the rounded edges of the isolated vehicle is also lowered but the net effect is a drag decrease. Although the general flowfield looks similar when comparing the three cases from above some differences can be noted. This vertical misalignment causes more flow to exit from the top of the trailing model compared to aligned case. The flow that is coming from the

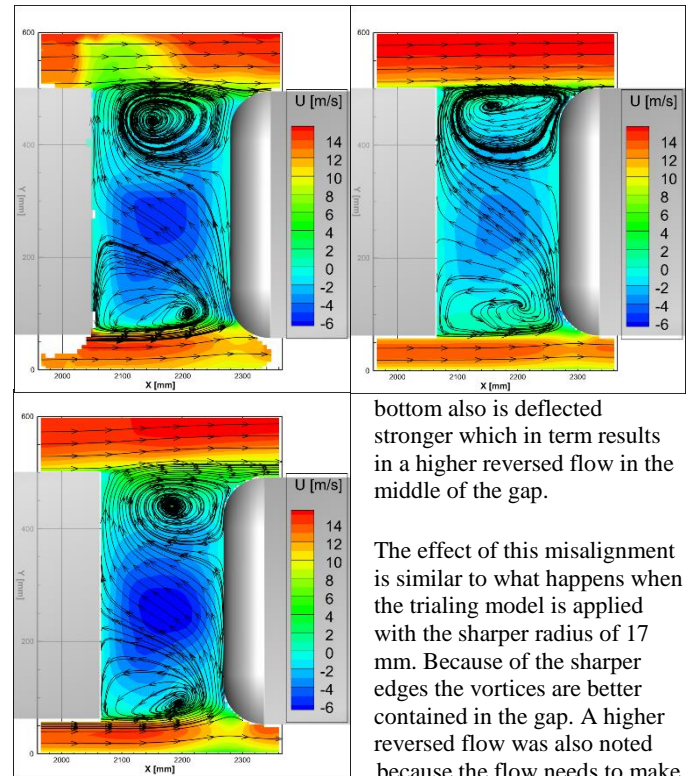


Figure 15. Time-averaged streamlines with contours of x-velocity in the vertical centre plane of the R68-R68 platoon at 0.10 s/L
Top left: experiment, top right aligned simulation, bottom left misaligned simulation.

bottom also is deflected stronger which in term results in a higher reversed flow in the middle of the gap.

The effect of this misalignment is similar to what happens when the trailing model is applied with the sharper radius of 17 mm. Because of the sharper edges the vortices are better contained in the gap. A higher reversed flow was also noted because the flow needs to make a sharper turn to stay in the gap. The higher drag decrease for the trailing model is due to the drop in stagnation pressure which in this case makes up more of the drag for the isolated model compared to the baseline configuration with a radius of 68 mm.

In this platoon configuration the unsteady forces of the leading model are similar to those of the single model but those of the trailing model are affected. Figure 16 illustrates the PSD of the drag and sideforce for the trailing models in the three configurations. For the baseline configuration a peak in the drag force can be seen at a Strouhal number of 0.102 its magnitude is only slightly higher compared to the isolated model. For the sideforce this is not the case here the peak at $St = 0.132$ is 3.5 times as high. When the sharper radius is applied the drag force fluctuates at the same Strouhal number as the baseline platoon at a slightly higher amplitude. The peak in the sideforce has been greatly reduced. For the misaligned configuration the amplitudes in drag and sideforce are much higher about 2 and 1.5 compared to the baseline platoon.

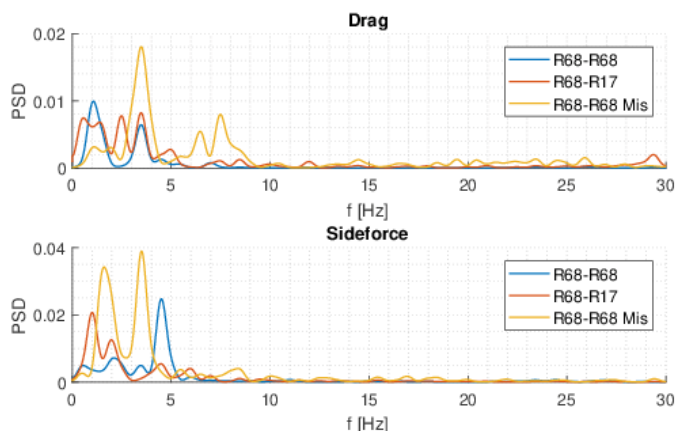


Figure 16. PSD of the drag and sideforce of the trailing model in a platoon at 0.10 s/L, PowerFLOW

These force variations are due to the pressure fluctuations that exist in the gap between the two models. The lower sideforce variation for the R68-R17 platoon comes from the fact that the flow is better contained in the gap and less area is exposed to the sides. For the misaligned platoon the fluctuations are highest because the flow in the gap is contained less well.

Middle intervehicle distance: 0.45 s/L

At the middle intervehicle distance of 0.45 times the vehicle length again three simulations were performed for which the drag results are shown in figure 17.

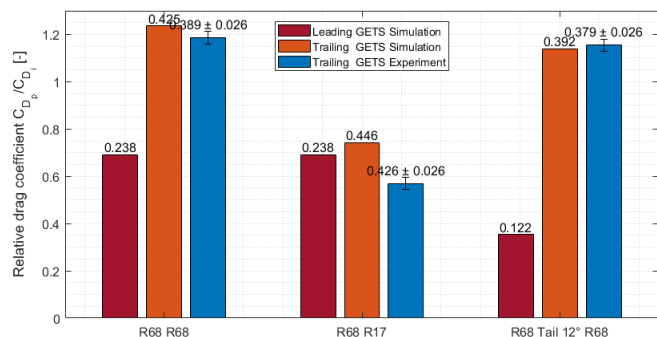


Figure 17. Numerical and experimental drag coefficient of the platoons at 0.45 s/L.

Here also the baseline platoon, one with sharper radius for the training model were simulated and an additional configuration of the baseline platoon where a tail of 12° was applied to the leading model was added. From this figure it can be seen that at this distance not all models in the platoon benefit from the configuration. The trailing model where the largest radius of 68 mm is applied has a drag increase of 24% and 14% for the baseline platoon and platoon with tail respectively. The trailing model with a radius of 17 mm does see a drag decrease. 26% less drag is generated compared to the isolated model. All the leading models do see a drag decrease 31% for the first two platoons and 65% for the last one. This last one is due to the combination of the tail and the platoon. For the experimental data also similar trends can be seen as for the data coming from the simulation. The drag increases and decreases are +17, -44 and +14%. The absolute differences are 36, 20 and 13 counts. The differences in relative and absolute drag can be attributed to a lateral alignment error for the baseline platoon. For the one where the sharpest radius

was applied this is due to the large difference in drag that was seen for the single GETS model with the sharp radius.

Again most of the drag from the leading model is reduced by the rear. The changes for the trailing model are also coming from the front. For the model with the sharpest radius there is a reduction in both suction and stagnation pressure, but the net effect causes a drag reduction. For the other two configurations this is not the case. Here the suction caused by the rounded edges has vanished completely this combined with the reduced stagnation pressure is not enough to result in a drag reduction. This phenomenon can be further explained by looking at the flowfield given in figure 18 and 19.

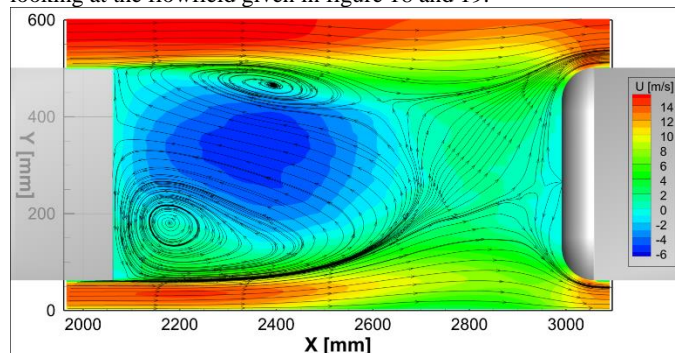
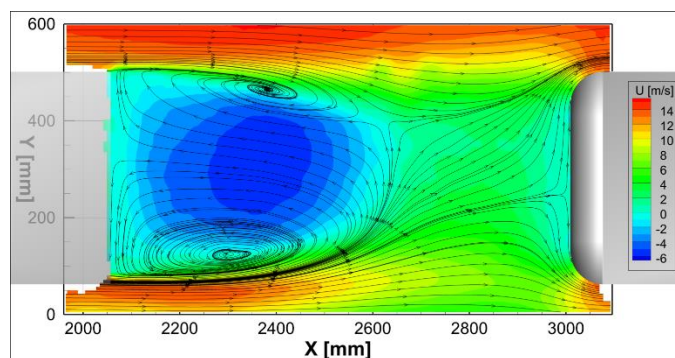


Figure 18. Time-averaged streamlines with contours of x-velocity in the vertical centre plane of the R68-R68 platoon at 0.45 s/L Top experiment bottom simulation.

Compared to the smaller intervehicle distance the wake structure at this distance has developed much more and starts to resemble that of the isolated model. Its main features are two main vortices and a saddle point located near the top of the model. In the wake structure a large region of reversed flow exists its magnitude is lower than that of the isolated model which causes a higher base pressure. The velocity in front of the trailing model is also greatly reduced. This leads to a lower stagnation pressure on one hand but also has an undesirable consequence for the rounded edges of the model. Due to the lower velocity seen by the rounded edges the flow is only accelerated to a value just below the free-stream velocity. This means that no negative pressure is formed on the rounded edges as was detected in the previous paragraphs. This lack of suction explains the drag increase experienced by the trailing model.



A similar result can be seen in figure 18 where the flowfield is shown when a tail is applied to the leading model. First of all the magnitude of the reversed flow has been reduced even more due to the tail which guides the flow.

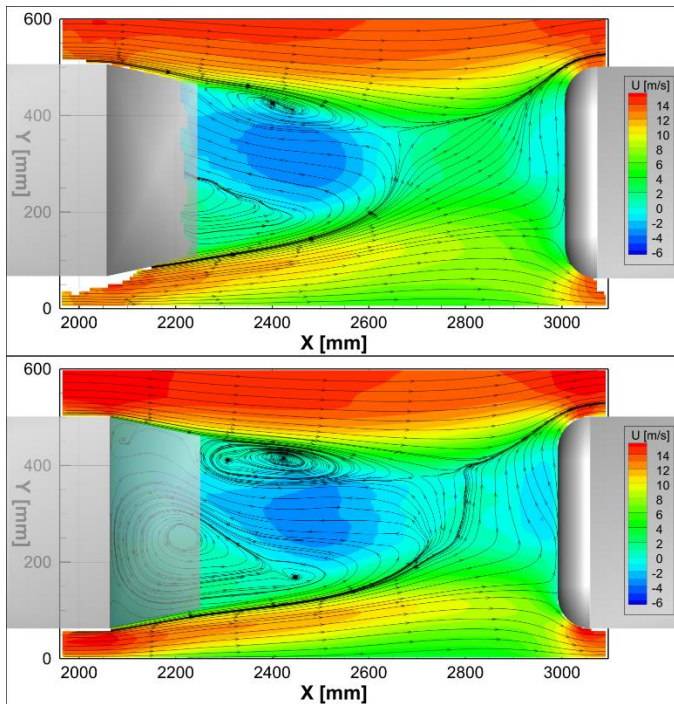


Figure 19. Time-averaged streamlines with contours of x-velocity in the vertical centre plane of the R68-12°-R68 platoon at 0.45 s/L. Top experiment bottom simulation.

This makes the wake region smaller which means that the air flowing over the rounded edges has a higher velocity and creates slightly more suction which leads to a smaller drag increase.

Whereas the force variation at 0.10 s/L was small at this distance some significant increases were seen especially for the models where no tail was applied to the trailing model.

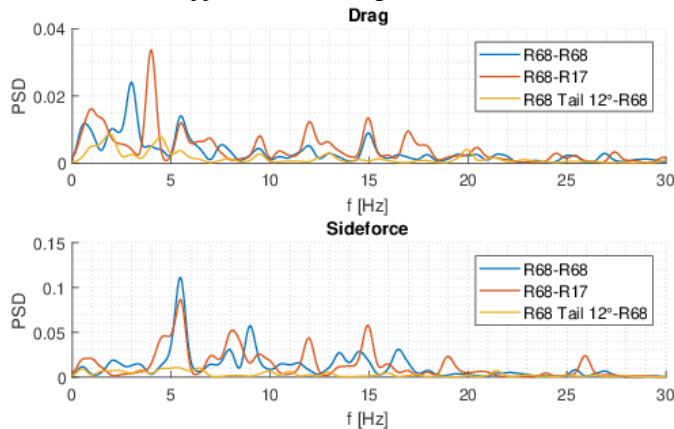


Figure 20. PSD of the drag and sideforce of the trailing model in the platoon at 0.45 s/L.

Figure 20 is illustrating this by presenting the PSD for the drag and sideforce. For the baseline platoon (R68-R68) the drag and sideforce fluctuate at a Strouhal number of 0.088 and 0.160. The magnitude of these peaks is twice and 6.5 times a high as the ones for the isolated model. The cause of these is the return of vortex shedding because of the more developed wake structure. These vortices impact the front of the trailing model which causes these fluctuations. For the configuration where the trailing model has a sharper radius the force fluctuations occur at $St = 0.117$ and 0.160. The magnitude of the drag force is higher and the magnitude of the sideforce is lower compared

to the baseline platoon. This can be attributed to the way the vortices are received by the model. Because of the sharper radius the vortices are not deflected that easily leading to a higher drag force fluctuation. Next to this also less area is exposed to the sides which explains the lower sideforce fluctuations. For the last configuration in this plot the force fluctuations have been greatly diminished. It was already seen that effect of a tail of 12° on a single model reduced the force fluctuations. This is also the cause of the lower fluctuations for this configuration.

Besides the configurations where both data from simulations and the experiment was available more configurations were tested in the wind tunnel. Figure 21 shows the difference in drag compared to the baseline isolated model; the drag difference ΔC_D is $C_{d \text{ trailing}} - C_{d \text{ isolated}}$.

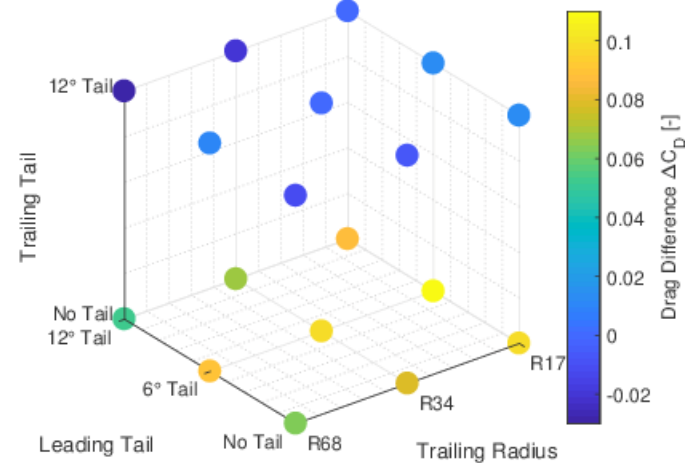


Figure 21. Experimental drag difference between the baseline isolated model and the trailing model in the platoon at 0.45 s/L. $\Delta C_D = C_{d \text{ trailing}} - C_{d \text{ isolated}}$. Positive values are drag increases, negative values drag decreases.

During these measurements three variables were changed namely the tail of the leading model, the front edge radius of the trailing model and the tail of the trailing model. For the tail of the leading model the options were no tail, a tail of 6° or one of 12°. For the trailing model a radius of 68, 34 or 17 mm could be chosen and for the trailing tail the two options were no tail or one of 12°. This lead to a total of 18 configurations. The highest drag is achieved by the configuration with the leading tail of 6°, the sharpest radius of 17 mm and no tail for the trailing model. The lowest drag configuration is the one where both models have a tail of 12° and the bluntest radius of 68 mm is applied to the trailing model.

Applying a tail of 12° to the trailing model is always a good idea. All the configurations benefit when a tail is added to the trailing model. Adding a tail to the leading model however is not always a good idea. For every configuration the addition of a 6° tail increases the drag compared to when no tail was added. Adding a tail of 12° however is reducing the drag of every configuration again. It is assumed that when a tail of 6° is added the drag increase is caused by a smaller drag reduction due to the incoming flow of higher velocity compared to when no tail is applied. This faster flow also means more suction is created. The assumption is that this effect is stronger when the tail of 12° is applied which then causes the overall drag decrease. When it comes to front radius the most streamlined model still has the lowest drag. Additionally it is also visible that with a lower front edge radius the model becomes less sensitive to changes made at the rear of the leading model and that the achieved drag reductions decrease with

decreasing radius. This is because for a sharper radius the thrust force generated by the front is of less importance since most of the drag reduction is gained from the reduced stagnation pressure which is influenced less by the addition of tails.

Largest intervehicle distance: 0.91 s/L

At the last and largest separation of 0.91 s/L only simulations were performed. The two configurations that were simulated were the baseline platoon and one where the sharper radius is applied to the trailing model, their results are presented in figure 22.

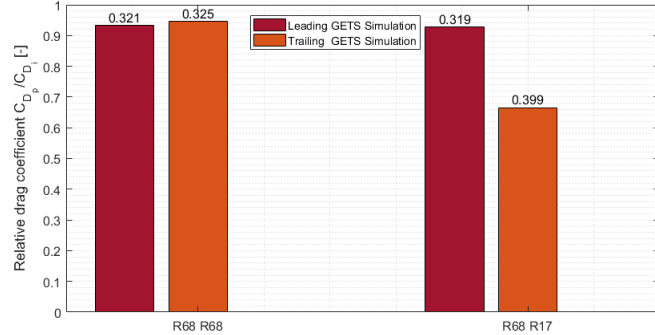


Figure 22. Numerical drag coefficient of the platoons at 0.91 s/L.

At this distance the baseline platoon only benefits a few percentages, 7 and 5% of the drag is reduced for the leading and trailing model. This is similar to what was found by Gheysens [9] where a drag reduction of 6% was seen for the leading model. For the other configurations the drag of the leading model is also reduced by 7%. For the trailing model a much higher reduction is seen, 34%. Again this is similar to the value of 37% found by Gheysens [9].

For the leading model most of the drag is reduced from the rear surface. For the trailing model of the baseline platoon the drag is mostly reduced by the sides and supports. For the front a very small increase in drag can even be seen. This is due to the diminished suction from the rounded edges and the reduced stagnation pressure which in this case almost cancel each other out. For the model with the sharper radius applied most of the drag reduction is coming from the front surface. In this case the reduction of stagnation pressure together with the small decrease in suction means that a lot more drag is reduced.

At this distance the effect of the vortices being shed by the leading model have no effect anymore on the trailing model and the force fluctuations have returned to the level that was also seen for the isolated model.

Critical intervehicle distance

Having discussed the results at all three intervehicle distances the effect of intervehicle distance on more rounded and sharp front edge radii can be seen. In figure 23 the absolute drag coefficient of the trailing vehicle as well as the drag in isolation is given.

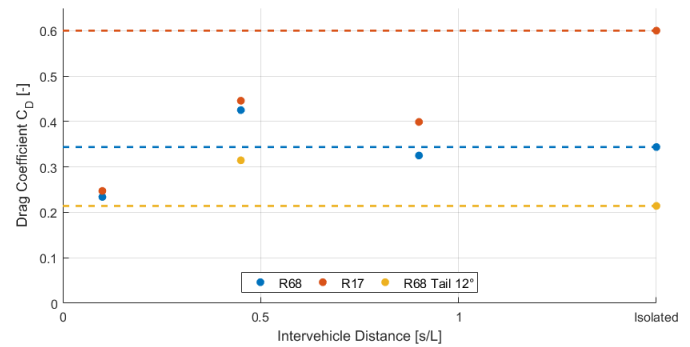


Figure 23. Absolute drag coefficient of platoon and isolated vehicle showing the critical intervehicle distance.

From this it is noted that for the model with the sharper radius the platoon configuration is always beneficial. This is due to the separation which was seen in isolation and does not occur or is reduced because of the velocity field of lower magnitude coming from the vehicle in front. For models where the flow is attached in isolation this is different. For these models the drag is not always reduced and there exists a critical separation distance at which the drag is increased. This drag increase is due to the reduced suction coming from the rounded edges of the model together with reduced stagnation pressure. Below this distance the reduction of the stagnation pressure is high enough to cause a drag decrease and above this distance the suction of the rounded edges has recovered to a high enough value to also cause a drag decrease.

Conclusion

The aim of this work was to provide more insight into the flow field that exists between two vehicles in a platooning configuration at very close separation distances. A numerical and experimental investigation was performed on GETS models both in isolation and in a two vehicle platoon.

For the single baseline model, the results from the simulation and experiment were very comparable. The addition of sharper front edge radii leads to higher drag. However a difference in simulation and experimental results was seen due leading edge flow separation occurring on the wind tunnel model. When tails are added to the single model the drag decreases with increasing tail angle. Unsteady force oscillations also follows this trend.

At the smallest intervehicle distance the largest drag reductions were noted. For the trailing model the sharper the radius the larger the drag reduction. The general flow path between the two models is given by an S-shape flow enters from the bottom and ends up in the lower vortex, stagnates on the rear or front or ends up in the upper vortex where it can flow out of the gap again. A small increase in force variation for the trailing model was also noted.

For the middle intervehicle distance the leading model always experiences a drag reduction. For the trailing model this is not the case. When the largest radius is applied the drag is increased compared to the isolated case, this is due to the loss of suction coming from the rounded edges. When the sharpest radius is applied this is not the case. The reduction in stagnation pressure overcomes this loss in suction resulting in a drag decrease. The addition of tails to the trailing model always results in a larger drag decrease. When these are applied to the leading model this is not always the case. The

wake structure at this distance resembles that of the isolated case with a large and small vortex and saddle point. Vortices shed from this wake impact the trailing model and enlarge the unsteady force behavior.

At the final distance the effect of the platoon has been greatly reduced. For the baseline only a few percent drag reduction was shown. For the model with sharper radius the drag reduction was larger due to its larger stagnation surface. At this distance the wake structure has returned to that of the model in isolation. The vortices shed by the leading model are too weak at the trailing model to influence the unsteady force behavior.

Models that already have a well designed front-end can have a drag increase while in a platoon configuration. This behaviour only occurs at a critical separation distance. This should be investigated further if the separation distance found here is the only one where this occurs or if there are others. Models with bad front-end designs always benefit more both in absolute and relative numbers while driving in a platoon.

Next to the critical separation distance further research should be done on the effect of platoons when a yaw angle is applied. Besides this from literature it was found that cooling orifices could have a reduced mass flow in a platooning configuration. This should be studied as well for these types of models.

References

1. Muncrief, R., Sharpe, B., "Overview of the heavy-duty vehicle market and CO2 emissions in the European Union," Technical report, The International Council on Clean Transportation (ICCT), 2015.
2. Miller, J.D., Façanha, C., "The state of clean transport policy a 2014 synthesis of vehicle and fuel policy developments," Technical report, The International Council on Clean Transportation (ICCT), 2014.
3. Thorsten, F., Turney, J., "Aerodynamics of Commercial Vehicles." The Aerodynamics of Heavy Vehicles III Lecture Notes in Applied and Computational Mechanics, August 20, 2015, 195-210. http://dx.doi.org/10.1007/978-3-319-20122-1_12.
4. McAuliffe, B., "Improving the aerodynamic efficiency of heavy duty vehicles: wind tunnel test results of trailer-based drag-reduction technologies," Report, National Research Council Canada. Aerospace, July 22, 2015.
5. Van Raemdonck, G., "Design of Low Drag Bluff Road Vehicles," PhD thesis, Delft University of Technology, 2012.
6. Hyams, D., Sreenivas, K., Pankajakshan, R., Nichols, S. et al., "Computational Simulation of Model and Full Scale Class 8 Trucks with Drag Reduction Devices." Computers & Fluids 41, no. 1 (February 2011): 27-40. doi:10.1016/j.compfluid.2010.09.015.
7. Hammache, M., Michaelian, M., and Browand, F., "Aerodynamic Forces on Truck Models, Including Two Trucks in Tandem," SAE Technical Paper 2002-01-0530, 2002, <https://doi.org/10.4271/2002-01-0530>.
8. Mihelic, R., Smith, J., and Ellis, M., "Aerodynamic Comparison of Tractor-Trailer Platooning and A-Train Configuration," SAE Int. J. Commer. Veh. 8(2):740-746, 2015, <https://doi.org/10.4271/2015-01-2897>.
9. Gheysens, T., "Aerodynamic analysis of a platoon of bluff bodies subjected to cross wind," Master's thesis, Delft University of Technology, 2016.

10. Chen, H. "Extended Boltzmann Kinetic Equation for Turbulent Flows." Science 301, no. 5633 (2003): 633-36. doi:10.1126/science.1085048.
11. Bhatnagar, P. L., E. P. Gross, and M. Krook. "A Model for Collision Processes in Gases. I. Small Amplitude Processes in Charged and Neutral One-Component Systems." Physical Review 94, no. 3 (1954): 511-25. doi:10.1103/physrev.94.511.
12. Exa Corporation. Powerflow user's guide, 2017b.
13. SAE., "Guidelines for Aerodynamic Assessment of Medium and Heavy Commercial Ground Vehicles Using Computational Fluid Dynamics," Sep 2013. URL https://doi.org/10.4271/J2966_201309.
14. van Tilborg, F., "Flow analysis between two bluff bodies in a close distance platooning configuration," Master's thesis, Delft University of Technology, 2018.
15. Alons, H.J., "OJF External Balance". Technical report, National Aerospace Laboratory (NLR), 2008.
16. Scarano, F., Ghaemi, S., Caridi, G., Bosbach, J. et al., Uwe Dierksheide, and Andrea Sciacchitano. "On the Use of Helium-filled Soap Bubbles for Large-scale Tomographic PIV in Wind Tunnel Experiments." Experiments in Fluids 56, no. 2 (February 11, 2015). doi:10.1007/s00348-015-1909-7.
17. Soloff, S. M., Adrian, R.J., and Liu, Z-C, "Distortion Compensation for Generalized Stereoscopic Particle Image Velocimetry." Measurement Science and Technology 8, no. 12 (1997): 1441-454. doi:10.1088/0957-0233/8/12/008.
18. Wieneke, B. "Volume Self-calibration for 3D Particle Image Velocimetry." Experiments in Fluids 45, no. 4 (2008): 549-56. doi:10.1007/s00348-008-0521-5.
19. Schanz, D., Gesemann, S., and Schröder, A., "Shake-The-Box: Lagrangian Particle Tracking at High Particle Image Densities." Experiments in Fluids 57, no. 5 (2016). doi:10.1007/s00348-016-2157-1.
20. Jux, D., "Robotic volumetric particle tracking velocimetry by coaxial imaging and illumination," Master's thesis, Delft University of Technology, 2017.
21. Van Raemdonck, G., Van Tooren, M., "Time averaged phenomenological investigation of a wake behind a bluff body," presented at International Colloquium on: Bluff Bodies Aerodynamics & Applications Milano, Italy, July, 20-24 2008.
22. Khalighi, B., Zhang, S., Koromilas, C., Balkanyi, S. et al., "Experimental and Computational Study of Unsteady Wake Flow Behind a Bluff Body with a Drag Reduction Device," SAE Technical Paper 2001-01-1042, 2001, <https://doi.org/10.4271/2001-01-1042>.
23. Krajnović, S. and Davidson, L., "Large-Eddy Simulation of the Flow Around a Ground Vehicle Body," SAE Technical Paper 2001-01-0702, 2001, <https://doi.org/10.4271/2001-01-0702>.
24. Roberts, J., Mihelic, R., and Roeth, M., "Two truck platooning," Confidence report, North American Council for Freight Efficiency, 2016.

Contact Information

Frank van Tilborg
frank.van.tilborg@hotmail.com

Contact details for the main author should be included here. Details may include mailing address, email address, and/or telephone number (whichever is deemed appropriate).

Acknowledgments

If the Acknowledgments section is not wanted, delete this heading and text.

Definitions/Abbreviations

GETS Generalized European Transport System

CVV Coaxial Volumetric Velocimetry